

# ACCURACY MODEL FOR PHASE NOISE MEASUREMENTS\*

F. L. Walls, C.M. Felton, A.J.D. Clements  
National Institute of Standards and Technology  
Boulder, CO 80303  
and  
T.D. Martin  
Gravity Research Institute  
Boulder, CO

## Abstract

We have recently completed a new modular system for accurate measurements of phase noise in oscillators, amplifiers, frequency synthesizers, and passive components. This new system is capable of measuring the phase noise at carrier frequencies from 5 MHz to 1.5 GHz, 1.5 to 26 GHz, and 33 to 50 GHz. Other frequency ranges can be measured using external mixers to convert the signals into one of the above frequency ranges. The analysis bandwidths vary from 0.1 Hz to 10% of the carrier frequency up to a maximum of about 1 GHz. Extensive internal calibration of the system is used to correct for all gain variations with analysis frequency including phase-locked-loop and cable-loss effects. We have also included a precision noise source to calibrate the spectral density functions of the spectrum analyzers. As a part of this program we have developed a method for determining the biases in the various spectrum analyzers as a function of noise type and the confidence of the spectral density estimates. We also investigate the effect of amplitude noise and phase delays on phase noise measurements. The combination of all these features makes it possible, under favorable conditions, to measure phase noise in various signal handling components and sources to an accuracy of 1 dB over very wide analysis bandwidths. Detailed descriptions of the new calibration procedures, including a sample table of uncertainties, are given. High accuracy determinations of phase noise can be used to compute accurate values of short-term, time-domain frequency stability.

## I. INTRODUCTION

We have developed a new concept for the measurement of phase noise offering much higher accuracy and bandwidth than was possible using previous approaches.<sup>1-4</sup>. This new approach makes it possible to measure phase noise over bandwidths that approach 10% of the carrier frequency (up to a maximum frequency of about 1 GHz) with an accuracy that exceeds 1 dB under most conditions. The wide bandwidths and the higher accuracy are necessary to adequately characterize new equipment used in

---

\*Contribution of the U.S. Government; not subject to copyright.

very wide bandwidth communication, navigation, and measurement systems. To achieve these new goals, it was necessary to develop a method to calibrate virtually every aspect of the measurement process, to reconsider the effects of residual amplitude noise, and to examine the confidence of spectral estimates for non-white noise.

## II. MODEL OF A NOISY SIGNAL

Equation 1 shows the simple model of the signal of a source where the frequency fluctuations are very small compared to the average frequency,  $\nu_0$  and the fluctuations in the amplitude are very small compared to the average amplitude,  $V_o$ . The amplitude variations are incorporated into  $\epsilon(t)$  and the phase or frequency fluctuations are incorporated into  $\phi(t)$ <sup>[5,6]</sup>:

$$V(t) = [V_o + \epsilon(t)]\cos[2\pi\nu_0 t + \phi(t)]. \quad (1)$$

The phase noise of such a source is often expressed in terms of  $S_\phi(f)$ , the spectral density of phase fluctuations.  $S_\phi(f)$  can be understood as the one-sided, mean-squared phase fluctuation,  $\delta\phi^2(f)$ , measured at a Fourier frequency separation,  $f$ , from the carrier in a measurement bandwidth BW.

$$S_\phi(f) = \frac{\delta\phi^2(f)}{\text{BW}} \quad (\text{rad}^2/\text{Hz}) \quad 0 < f < \infty. \quad (2)$$

Equations 3 and 4 show the relationship between  $S_\phi(f)$  and several commonly used expressions for frequency or phase fluctuation.  $\mathcal{L}(\nu_0 - f)$  is the single-sideband phase noise at a frequency,  $f$ , below the carrier while  $\mathcal{L}(\nu_0 + f)$  is the single sideband noise at a frequency,  $f$ , above the carrier. There may be conditions under which the upper sideband is not equal to the lower sideband.  $S_y(f)$  is the spectral density of fractional frequency fluctuations.

$$S_\phi(f) = \mathcal{L}(\nu_0 - f) + \mathcal{L}(\nu_0 + f) \quad (3)$$

$$S_y(f) = \frac{f^2}{\nu_0^2} S_\phi(f) \quad 0 < f < \infty \quad (4)$$

These measures fully characterize the random variations of the phase of a precision source. The time domain characterization of the frequency fluctuations are usually expressed in terms of the Allan variance,  $\sigma_y^2(\tau)$ , or the modified Allan variance, Mod  $\sigma_y^2(\tau)$ . Both variances can be accurately determined by an integration of  $S_y(f)$  or equivalently  $S_\phi(f)$  as shown below, where the measurement time is  $n$  times the minimum measurement time,  $\tau_0$ , and  $f_h$  is the measurement bandwidth. An accuracy of 1 dB in determining  $S_\phi(f)$  corresponds to about 10% accuracy in determining  $\sigma_y(\tau)$  or Mod  $\sigma_y(\tau)$ . Numerical integration techniques have been used to extend earlier work and calculate the ratio of Mod  $\sigma_y^2(\tau)$  to  $\sigma_y^2(\tau)$  for all the common noise types found in oscillators and measurement systems as shown in Figure 1<sup>[7-11]</sup>. This makes it possible to transform from  $\sigma_y(\tau)$  to Mod  $\sigma_y(\tau)$  and back for virtually any value of  $n$ . Mod  $\sigma_y(\tau)$  averages the high-frequency-phase-noise components of white-phase and flicker-phase noise faster than  $\sigma_y(\tau)$ . This can be very useful in measuring the long-term performance of a source which has high frequency noise components<sup>[4-9]</sup>. The inversion of  $\sigma_y(\tau)$  or Mod  $\sigma_y(\tau)$  to obtain  $S_\phi(f)$  has relatively poor precision due to the integral nature of the time domain measures. These inversions are

$$\sigma_y(n\tau_0) = \left[ 2 \int_0^{f_h} S_y(f) \frac{\sin^4(\pi f n\tau_0)}{(\pi f n\tau_0)^2} \right]^{1/2} \quad \text{and} \quad (5)$$

$$\begin{aligned} \text{Mod}\sigma_y(n\tau_0) = & \left[ \frac{2}{n^4 \pi^2 \tau_0^2} \left[ n \int_0^{f_h} \frac{S_y(f)}{f^2} \sin^4(\pi f n\tau_0) df \right. \right. \\ & \left. \left. + 2 \int_0^{f_h} \sum_{k=1}^{n-1} (n-k) \frac{S_y(f)}{f^2} \cos(2\pi f k\tau_0) \sin^4(\pi f n\tau_0) df \right] \right]^{1/2}. \end{aligned} \quad (6)$$

Equation (6) can be simplified<sup>[7]</sup> to:

$$\text{Mod}\sigma_y(n\tau_0) = \left[ \frac{2}{n^2 (\pi n\tau_0)^2} \int_0^{f_h} S_y(f) \frac{\sin^6(\pi f n\tau_0)}{f^2 \sin^2(\pi n f \tau_0)} df \right]^{1/2}. \quad (7)$$

Generally, the effect of the time variations on the signal amplitude,  $V(t)$ , as characterized by the power spectral density of amplitude fluctuations,  $S_v(f)$ , are ignored in the measurement of  $S_\phi(f)$ . However,  $S_v(f)$  often sets the lower limits for the measurement of added noise in devices and in determining the noise floor of measurement systems.  $S_v(f)$  is given by

$$\begin{aligned} S_v(f) = & \frac{\delta\epsilon^2(f)}{V_0^2 \text{BW}} \quad (\text{rel to carrier/Hz}) \quad \text{or} \\ & 10 \log S_v(f) \quad (\text{dBc/Hz}) \end{aligned} \quad (8)$$

where  $\delta\epsilon^2(f)$  is the mean-squared amplitude fluctuation measured at a Fourier frequency separation,  $f$ , from the carrier in a measurement bandwidth, BW.

### III. PHASE NOISE MEASUREMENT SYSTEM

Figure 2 shows a block diagram of our new modular phase-noise-measurement system for measuring phase noise in oscillators, amplifiers, frequency synthesizers and other devices. As presently configured, three front end units cover the bands of 5 to 1500 MHz, 1.5 to 26 GHz, and 33 to 50 GHz. Other frequency ranges can be easily added by the installation of cables which carry the appropriate reference frequencies as discussed below, or by using external mixers to heterodyne the frequencies into the range of one of the three present front ends. Using this latter approach makes it possible to extend the range to cover the entire millimeter range and most laser frequencies as well.

All three front ends feature directional couplers for continuous monitoring of the frequency or power of the input signals. They also have internal phase shifters for use in making measurements of the noise floor or the phase added by signal handling components. The power meter covers 100 kHz to 50 GHz while the counter covers 0.001 Hz to 26 GHz. The modulation reference source covers 0.1 Hz to 1 GHz. The low-phase-noise frequency reference has outputs at 5, 10, 100,  $N \times 500$  MHz ( $1 \leq N \leq 30$ ), 10.6 GHz, 21.2, GHz and 42.4 GHz. There is also a low-noise frequency synthesizer which covers 10 kHz to 1.28 GHz.

The system can be run manually from the front panels of the various instruments or run from an AT-compatible microprocessor. The microprocessor makes it easy to perform a wide variety of calibrations, to correct for variations in the various instruments over the frequency range of interest. As with previous systems, a mixer is used to transform phase variations to voltage variations that are measured by various spectrum analyzers<sup>[1-4]</sup>. The signal from the mixer in each of the front ends is switched to a common amplifier that has several output channels. Each is optimized to drive a particular measurement instrument. There are three spectrum analyzers, a 100 MHz digital oscilloscope and a multipurpose counter. By far the most difficult task is to determine, with an accuracy of 0.5 dB, the sensitivity of the mixer for converting small phase variations to voltage variations for Fourier frequencies from dc to about 1 GHz. In previous approaches the mixer calibration was accomplished with amplifiers that were very flat with frequency and by calibrating the mixer conversion sensitivity using the beat frequency method<sup>[1,2]</sup>. This is possible for Fourier frequencies which are very small compared to the carrier, but extremely difficult at higher Fourier frequencies due to the dependence of the reactive impedance of the mixers on termination and source characteristics<sup>[2]</sup>. Our new method overcomes this difficulty.

#### IV. BASIC MEASUREMENT PROCESS

The first step in the measurement of phase noise between two oscillators is to adjust the input drive levels of the signal and reference channels to between +13 and +23 dBm. Next we use the beat frequency method to calibrate the absolute sensitivity for transforming small variations in phase to voltage variations at the output of the scope channel shown in Figure 3. The period of one beat cycle ( $2\pi$  rad) is determined using the digital oscilloscope. The oscilloscope is then used to digitize the beat signal and determine the average slope at approximately  $\pm 0.05$  radians of the zero crossing. The oscilloscope channel uses a relatively low-gain (22 dB) operational amplifier with high slewing rate and dynamic range. This measurement is done at a low beat frequency where the frequency response of both the mixer and the amplifier is constant. The sensitivity at the output of the oscilloscope channel is just

$$k_d = \text{slope (V/s)} T(s)/(2\pi) \quad (\text{volts/rad}). \quad (9)$$

We measure both the positive-going and the negative-going zero crossings to verify that they are equal to better than 10%. If they are not the same the mixer may be damaged or there may be significant injection pulling which would invalidate the slope measurements. The injection pulling can be reduced by increasing the beat frequency. When the beat signal is noisy, it is averaged with the digital oscilloscope to improve the precision of the measurement. Typically, this measurement is accurate to better than 1%, which corresponds to  $\pm 0.09$  dB in the determination of  $S_\phi(f)$ .

The tuning sensitivity of one of the oscillators is then determined using the counter and a programmable, voltage-bias source. This measurement, along with the determination of  $k_d$ , is used to calculate the appropriate gain and integration times to close the phase lock loop (PLL). The dc output voltage from the mixer, divided by  $k_d$ , yields the phase deviation from quadrature. This phase offset is continuously monitored to verify that it does not exceed 0.1 rad. If this limit is exceeded, an error message is sent to the operator. The phase noise data are also tagged with the peak phase deviation during the entire run. This is intended to help in the detection of large phase excursions during the measurements which would invalidate the data.

Once the phase lock is executed and the phase deviations from quadrature are verified to be less than  $\pm 0.1$  rad, a special phase modulator is used to determine the relative gains of all the amplifiers over the entire range of Fourier frequencies of interest. A schematic diagram of the phase modulator, which is used in each front end to generate phase modulation on the reference carrier signal, is shown in Figure 4. A small portion of the input carrier signal is coupled into a processing channel using a directional coupler. This signal is phase shifted, bi-phase amplitude-modulated using a double balanced mixer, and reinserted into the carrier. If the phase shift is such that the reinserted signal is at precisely  $90^\circ$  to the carrier, the resulting modulation is phase modulation with negligible amplitude modulation. This is illustrated by the vector diagram in Figure 2. This special condition of nearly pure phase modulation is obtained in practice by monitoring the signal after the phase modulator and actively adjusting the phase shift until the amplitude modulation is minimized. This eliminates the need to actually measure the phase shift. The adjustment need only be made at the beginning of a measurement, since it is very stable.

Figure 5 shows the variation in the amplitude of the phase modulation tones introduced by three phase modulators of the type shown in Figure 4 as a function of the frequency of the modulation. This figure shows that it is possible to insert phase modulation tones (on the carrier) that are constant in amplitude to  $\pm 0.5$  dB from dc up to 5 to 40% of the carrier frequency. The difference in performance is evidently related to the standing-wave ratio introduced by the components.

To calibrate the relative gains of the various measurement channels, the frequency of the modulation is swept over the range of Fourier frequencies of interest, and the response of the various measurement instruments is recorded. The ratio of the response of the instruments is then the relative gain. This corrects for frequency-dependent effects in the mixer and amplifiers, the effect of the PLL on the low frequency gains, cable losses, and even errors in the internal-voltage references of the instruments. Since the absolute response of the oscilloscope channel was determined above, using the beat frequency method, the sensitivity of all the other channels can be calculated. The repeatability of the measurement of the relative gains of the amplifiers and their measurement instruments is typically better than  $\pm 0.02$  dB up to 32 MHz and about  $\pm 0.2$  dB up to 0.5 GHz.

The spectral density function of the low-frequency spectrum analyzer is verified using the noise source shown in Figure 6 where the output is proportional to the Johnson noise from a metal-film resistor. The gains of the amplifiers are determined to 0.05 dB from the ratios of resistors. The noise density output is known to  $\pm 0.14$  dB from 20 Hz to 20 kHz. At higher frequencies the noise gain of the amplifiers becomes important and is compensated to 0.2 dB out to 100 kHz. Figure 7 shows a calibration of the spectral density function of the low-frequency spectrum analyzer for several different window functions<sup>[12]</sup>. The Hanning window has proven to be the most suitable for measuring noise while the "Flattened-Peak window" is best suited for the measurement of discrete peaks<sup>[12]</sup>. The primary uncertainty in the 20 Hz to 20 kHz region is the temperature;  $\pm 10$  K corresponds to  $\pm 0.14$  dB in the noise density. The effect of the input-noise current and added-noise voltage of the amplifier is determined by measuring the output-noise density for input terminations of  $10^5$  ohms, 220 pF in parallel with  $44 \times 10^6$  ohms and a short. This noise source can be injected into the output of the mixer and used with the relative gains to verify the measurement bandwidths of the other two spectrum analyzers.

The next step in the process is to measure the noise voltage on the three spectrum analyzers. This data is stored and later scaled by the relative gains and measurement bandwidths to obtain  $S_\phi(f)$ . The statistical confidence of the data is calculated using the method outlined previously<sup>[12]</sup>. For the low-frequency spectrum analyzer, which is a fast-Fourier-transform (FFT) device, the confidence

interval is virtually independent of the noise type (if the first few channels are neglected), and is given by

$$S = S_m \left(1 \pm \frac{1}{\sqrt{N}}\right), \quad (10)$$

where  $S$  is the true spectral density,  $S_m$  the measured spectral density, and  $N$  the number of independent samples averaged together. For the other spectrum analyzers, which use sweeping techniques, the confidence interval is roughly the square root of the ratio of the measurement bandwidth, before the detector, to the smoothing bandwidth. Accurate determinations of the confidence intervals for specific instruments can be obtained using<sup>[12]</sup>.

## V. CORRECTIONS FOR NOISE FLOOR, 3-CORNER HAT

The above procedure determines only the phase noise BETWEEN the two oscillators plus the noise floor of the measurement system, and does not, by itself, determine the noise of either oscillator. All we can say with certainty is that the phase noise of both oscillators is less than the measured value. To determine the phase noise of each unit, it is necessary to evaluate several additional terms which contribute to the apparent phase noise as shown in equation [11] and to measure both of the oscillators against another source of nearly equal noise performance.

$$\begin{aligned} S_\phi(f)_{|AB} &= \frac{[\Delta\phi_A(f) - \Delta\phi_B(f)]^2}{BW} + \frac{V_n^2(f)_{|\text{mixer}} + V_n^2|_{\text{Amp}} + [(V_n^2(f)_{|SA})/G^2]}{k_d^2} \\ &\quad + S_{VA}(f)\beta_A^2 + S_{VB}\beta_B^2, \end{aligned} \quad (11)$$

where  $[\Delta\phi_A(f) - \Delta\phi_B(f)]^2$  is the mean-squared phase fluctuations between the two ports of the mixer and the three  $V_n$  terms represent the amplitude noise of the mixer, the amplifier, and low pass filter, and the noise of the spectrum analyzer scaled by the amplifier gain.  $S_{VA}(f)$  is the amplitude noise of source  $A$  and  $\beta_A^2$  is the sensitivity of the mixer for converting amplitude noise into voltage noise at the output of the mixer.  $S_{VB}(f)$  represents similar terms for source  $B$ . For simple oscillators the amplitude noise of a source is generally no worse than the phase noise. This condition does not necessarily hold true for complex systems with automatic leveling circuits. Equation [11] can be simplified to

$$S_\phi(f)_{|AB} = S_{\phi A}(f) + S_{\phi B}(f) + \frac{V_n^2(f)}{k_d^2} + S_{VA}(f)\beta_A^2 + S_{VA}\beta_B^2. \quad (12)$$

The noise floor of the measurement system when driven by source  $A$  alone ( $A \equiv B$ ) is given by

$$S_\phi(f)_{|\text{Noise Floor}} = S_{\phi A}(2\pi f \tau_{\text{delay}})^2 + \frac{V_n^2(f)}{k_d^2} + S_{VA}(f)\beta_A^2 + S_\phi(f)_{|ps} \quad (13)$$

where  $S_\phi(f)_{|ps}$  is the added phase noise of the power splitter.

The term resulting from the phase difference between the two ports of the mixer drop out except for a new term which results from the  $90^\circ$  phase difference (between the ports) that is necessary for the

mixer to operate properly. This results in a dephasing of the phase noise of the source between the two ports of the mixer. The portion of the source appearing across the mixer increases as  $f^2$  and has the character of a delay-line, phase-noise-measurement system. This term is very important in wide-band, phase-noise-measurement systems, and is only 16 dB below the source noise for  $f = \nu_0/10$ , and  $\tau = 1/(4\nu_0)$ . The noise floor is also dependent on the amplitude noise of the delay source scaled by the conversion sensitivity of mixer.

Figure 8 shows one approach to measuring amplitude noise. The conversion sensitivity of the diode detector and the amplifier gain can be determined at a specific carrier frequency and power level using a substitute source that can be amplitude modulated. If the amplitude modulation signal is of the form,

$$V = V_0[1 + A_o \cos \alpha t] \cos \omega t,$$

where the relative power at the modulation frequency  $\alpha$  is  $A_o^2/2$  assuming  $A_o \ll 1$  and a linear detector. The signal detected at the spectrum analyzer is

$$\text{Output} = \frac{A_o^2}{2} G^2(\alpha) K_{AM}^2(\nu_0, V_0, \alpha),$$

where  $G^2(\alpha)$  is the square of the voltage gain of the amplifier at frequency  $\alpha$ , and  $K_{AM}^2(\nu_0, V_0, \alpha)$  is the conversion sensitivity of the diode.  $S_v(f)$  of the source of interest is then determined using the same  $G^2(f)$  and  $K_{AM}^2$ . The value of  $S_{VA}(f)$  determined by this approach is an upper limit since it does not directly determine the noise contribution of the diode or the amplifier.

The noise contribution of the amplifier can be determined by measuring the noise with no input signal. The measurements of the diode noise can sometimes be determined by comparing the results of several low-noise sources. These measurements are used to determine  $S_{VA}(f)$ ,  $S_{VB}(f)$  and estimate  $V_n(f)$ .

Table 1 shows the pair measurement of the phase noise of a frequency synthesizer against a low-noise quartz oscillator at 5 MHz. The amplitude noise was measured using the scheme shown in Figure 8. At low Fourier frequencies the amplitude noise is lower than the phase noise. However, at higher Fourier frequencies, the amplitude noise is higher than the phase noise. When the noise floor of the measurement system was measured, the noise floor was relatively high. By determining the mixer sensitivity for converting amplitude noise into output-voltage noise we could approximate the noise floor from the measured amplitude noise by  $S_v(f)|_A \beta_A^2$ . This shows that, in some circumstances, it is the amplitude noise and not the phase noise of the source that limits differential measurements such as the system noise floor or the phase noise added by a component.

The relative contributions of sources  $A$  and  $B$  to the pair measurement of equation 12 is determined by measuring both sources against another source,  $C$ . The phase noise of  $C$  should be roughly comparable or lower in phase noise than those of  $A$  or  $B$ . Equation 16 shows how these measurements can be combined with measurements of the noise floor and the amplitude noise to yield an unbiased estimate of  $S_\phi(f)$  for source  $A$ .

$$S_\phi(f)|_{AB} + S_\phi(f)|_{AC} + S_\phi(f)|_{BC} = 2S_{\phi A} + \frac{V_n^2(f)}{k_d^2} + 2S_{VA}(f)\beta_A^2. \quad (14)$$

Table 2 shows the results of a precise calibration of the phase noise of a 100 MHz frequency synthesizer against a low-noise quartz oscillator. The analysis covers the range from 32 Hz to 10 MHz or 10% of

the carrier frequency. The column showing modulation level indicates the modulation level detected on the two spectrum analyzers used for this calibration. The absolute sensitivity of the mixer multiplied by the gain of the oscilloscope channel at 100 Hz was 12.8 dB. The difference between the gain of the oscilloscope channel and the FFT channel was 14.3 dB. Combining these calibrations yields the values for the pair measurements of  $S_\phi(f)$ . Also listed is the amplitude noise of the frequency synthesizer (source A). The sensitivity of the mixer for converting the amplitude noise into output noise was -25.3 dB. When this is combined with the measured amplitude noise, the result is much below the measured phase noise. This result indicates that amplitude noise has negligible affect on the phase noise of these measurements. Direct measurements of the noise floor of the system, using the synthesizer as the driving source, indicate that the noise floor of the system also has negligible effect on the measured phase noise. Measurements of the phase noise against another source show that the phase noise of the synthesizer is 20 to 30 dB above the noise of the crystal oscillator (source B). The last column shows the final result of calibration. The uncertainties in the various steps of the calibration are listed in Table 3. The combination of these uncertainties is approximately  $\pm 1$  dB. The differences between columns 4 and 7 for Fourier frequencies of 50, 70, and 100 kHz are indicative of the statistical uncertainties of the noise spectral density measurements from the two channels.

## VI. CONCLUSION

We have outlined a new concept for the measurement of phase noise which features an accuracy of 1 dB under most conditions, and analysis bandwidths of approximately 10% of the carrier frequency up to a maximum of 1 GHz. A model which contains all the known contributions to the uncertainties in the measurement of phase noise is presented. This new approach uses a new type of ultra-flat phase modulator to determine all of the frequency dependent changes in the response of the mixer, the various amplifiers, cable losses, and even the internal calibration of the spectrum analyzers. The role of amplitude noise in the sources is also examined. It is shown that under some circumstances (especially differential measurements such as the noise floor of a system or the phase noise added by a signal processing component) the amplitude noise of the sources limits the ability to measure phase noise. It was also shown that when measuring the added phase noise of signal-handling components, the dephasing due to the 90° phase shift needed to operate the mixer in a linear region, limits the cancellation of the phase noise of the source. Combining all of these features, we are able, under most conditions, to determine the phase noise of signal sources and signal handling components to an accuracy of  $\pm 1$  dB.

## Acknowledgments

The authors wish to thank their many colleagues for helpful discussions on this topic, especially Dr. Tom Parker, Charles Stone, David Howe, Bob Temple, Michael Driscoll, Andrea DeMarchi, and David Allan. We also thank the Calibration Coordination Group of JCTG/CMT-JLC for support of this work.

## REFERENCES:

1. F.L. Walls, S.R. Stein, J.E. Gray, and D.J. Glaze, Design Considerations in State-of-the-Art Signal Processing and Phase Noise Measurement Systems, Proc. 30th Ann. SFC, 269-274 (1976). (Available from National Technical Information Service, Sills Building, 5285 Port Royal Road, Springfield, VA 22161.)
2. F.L. Walls and S.R. Stein Accurate Measurements of Spectral Density of Phase Noise in Devices, Proc. of 31st SFC, 335-343 (1977). (Available from National Technical Information Service, Sills Building, 5825 Port Royal Road, Springfield, VA 22161.)
3. A.L. Lance and W.D. Seal, Phase Noise and AM Noise Measurements in the Frequency Domain at Millimeter Wave Frequencies, from Infrared and Millimeter Waves, Ken Button Ed., Academic Press, NY 1985.
4. F.L. Walls, A.J.D. Clements, C.M. Felton, M.A. Lombardi, and M.D. Vanek, Extending the Range and Accuracy of Phase Noise Measurements, Proc. of the 42nd Ann. SFC, 432-441 (1988.)
5. J.A. Barnes, A.R. Chi, L.S. Cutler, D.J. Healey, D.B. Leeson, T.E. McGunigal, J.A. Mullen, Jr., W.L. Smith, R.L. Sydnor, R.F.C. Vessot, G.M. Winkler, Characterization of Frequency Stability, Proc. IEEE Trans. on I&M 20, 105-120 (1971.)
6. D.W. Allan, H. Hellwig, P. Kartaschoff, J. Vanier, J. Vig, G.M.R. Winkler, and N.F. Yannoni, Standard Terminology for Fundamental Frequency and Time Metrology, Proc. of the 42nd Ann. SFC, 419-425 (1988.)
7. F.L. Walls, J. Gary, A. O'Gallagher, R. Sweet and L. Sweet, Time Domain Frequency Stability Calculated from the Frequency Domain Description: Use of the SIGINT Software Package to Calculate Time Domain Frequency Stability from the Frequency Domain, NISTIR 89-3916.
8. D.W. Allan and J.A. Barnes, A Modified "Allan Variance" with Increased Oscillator Characterization Ability, Proc. of the 35th Ann. SFC, 470-475 (1981.)
9. P. Lesage and T. Ayi, Characterization of Frequency Stability: Analysis of the Modified Allan Variance and Properties of Its Estimate, IEEE Trans. on I&M, 1984, IM-33, 332-337.
10. V.P. Kroupa and L. Sojar, "Modified Allan Variance: Transfer Function and Practical Applications," CPEM 1984 Digest (Delft, the Netherlands.)
11. P. Tremblay in "Étude de l'Effet du Filiage du Signal sur la Caractérisation de la Stabilité de Fréquence," Thèse Université Laval, Quebec 1985.
12. F.L. Walls, D.B. Percival, and W.R. Ireland, Biases and Variances of Several FFT Spectral Estimators as a Function of Noise Type and Number of Samples, Proc. of 43rd Ann. SFC, 336-341 (1989.)

Table 1.

MEASUREMENTS OF  $S_\phi(f)$  @ 5 MHz

SYNTHESIZER VS OSCILLATOR

$f$ (Hz)	$S_\phi(f) _{AB}$ (dB Rel Rad <sup>2</sup> /Hz)	$S_v(f) _{AB}$ (dBc/Hz)	$S_v(f) _A \beta^2_A$ (dBc/Hz)	Measured Noise Floor (dBc/Hz)
32	-119.8	-126.0	$\approx$ -151.0	-154.0
100	-124.2	-127.0	$\approx$ -152.0	-154.0
1 K	-132.1	-132.0	$\approx$ -157.0	-158.0
10 K	-137.3	-133.0	$\approx$ -158.0	-158.0
100 K	-136.8	-133.0	$\approx$ -158.0	-158.0

Table 2.

MEASUREMENTS OF  $S_\phi(f)$  @ 100 MHz      SYNTHESIZER VS OSCILLATOR

0.050 to 32 MHz SA			0.1 Hz to 100 kHz SA			AM		NOISE		NOISE FLOOR		RESULT
f (Hz)	Noise (dBV/Hz)	Mod level (dBV)	$S_\phi(f)_{AB}$ (rad <sup>2</sup> /Hz)	Noise (dBV/Hz)	Mod level (dBV)	$S_\phi(f)_{AB}$ (rad <sup>2</sup> /Hz)	$S_{VA}(f)$ (dBc/Hz)	$\beta_A^2$ (dB)	$S_{VA}(f)$ (dBV/Hz)	$\beta_A^2$ (Rad <sup>2</sup> /Hz)	$S_\phi(f)_{AB}$ (Rad <sup>2</sup> /Hz)	
10 M	-99.1	-11.48	-148.0				-164					-148.0
5 M	-96.0	-10.85	-145.6				-160					-145.6
2 M	-94.8	-10.86	-144.3				-152					-144.3
1 M	-92.0	-11.33	-141.1				-150					-141.1
300 k	-84.7	-11.93	-133.2				-147					-133.2
100 k	-85.6	-14.63	-131.4	-107.2	-36.07	-131.5	-141	-25.3	-166	-163.0		-131.4
70 K	-88.4	-17.01	-131.8	-106.7	-34.94	-132.2						-132.0
50 k	-91.5	-20.10	-131.9	-105.8	-34.22	-132.0						-132.0
30 k				-105.5	-33.76	-132.1	-142		-167	-163.0		-132.1
10 k				-106.4	-33.38	-133.4	-147		-172	-163.5		-133.4
3 k				-105.8	-33.34	-132.9	-143		-168	-163.0		-132.9
1 k				-102.5	-33.49	-129.4	-144		-169	-163.0		-129.4
300				-102.4	-35.24	-127.6	-144		-169	-162.0		-127.6
100				-102.7	-41.79	-121.3	-139		-164	-159.0		-121.1
32				-102.0	-47.47	-114.9	-135		-160	-155.0		-114.8

Table 3. Table of Uncertainties

EFFECT	OFFSET	UNCERTAINTY (dB)
Spectral density function of 100 kHz Spect. Analy.	0	0.2
Spectral density function of 32 MHz Spect. Analy.	0	0.2
Determination of mixer sensitivity	See Table 2	0.1
Relative gains of amplifiers	See Table 2	0.02
Linearity of 100 kHz Spect. Analy.	0	0.15
Linearity of 32 Mhz Spect. Analy.	0	0.2
Statistical confidence of data	0	$\pm 1/(200)^*$
Contribution of system noise floor	0	0.05
unfolding 3 corner hat	0	0.1
Contribution of residual AM	0	0.05

## FUTURE PLANS

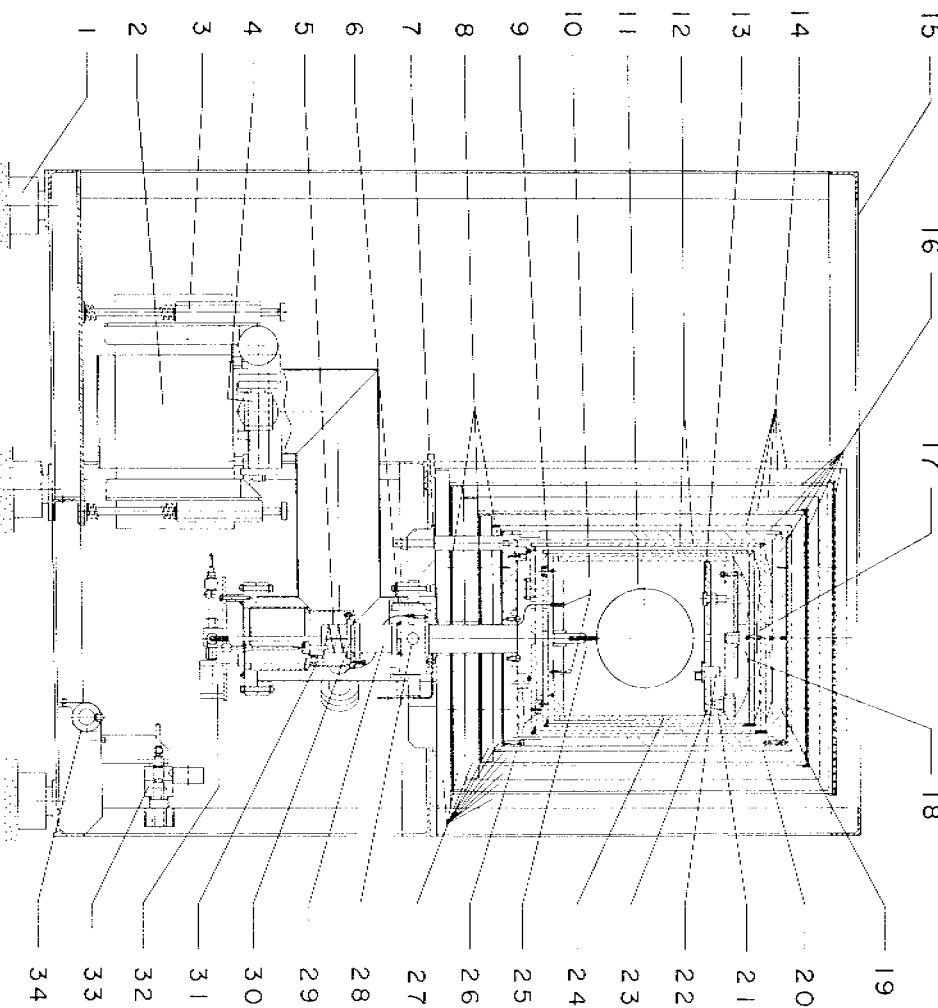
This paper is essentially a progress report on the development of the two new hydrogen masers. More comprehensive results will be reported at a later date, when all the final electronic circuits are in use. It is planned to obtain frequency stability data under free-running conditions and with the two different tuning systems before deciding which system gives rise to the best long term frequency stability. After this decision is made the masers will be incorporated into the NRC time scale as clocks.

## ACKNOWLEDGEMENTS

We would like to thank Mr. R. Cote and Mr. G.J. Trudeau for the mechanical construction of the masers, Mr. M. Kotler for assistance with the mechanical design, and Mr. W. Cazemier and Mr. J. Belanger for technical assistance with electronic circuits and mechanical assembly, respectively.

## REFERENCES

1. A. G. Mungall, D. Morris, H. Daams, and R. Bailey, *Metrologia* 4, 87–94 (1968).
2. J. Vanier, G. Racine, R. Kunski, and M. Picard, Proc. 12th Annual PTTI Applications & Planning Meeting, 807–824 (1980).
3. R. Kunski and J. Vanier, *J. Phys. E. Scientific Instr.* 15, 1207–1209 (1982).
4. C. Audoin, *Rev. Phys. Appl.* 16, 125–130 (1981).
5. D. Morris and K. Nakagiri, *Metrologia* 12, 1–6 (1976).
6. J. Vanier and R.F.C. Vessot, *Appl. Phys. Lett.*, 4, 122–123 (1964).
7. S.B. Crampton and H.T.M. Wang, *Phys. Rev. A* 12, 1305–1312 (1975).
8. D. Kleppner, H.C. Berg, S.B. Crampton, N.F. Ramsey, R.F.C. Vessot, H.E. Peters, and J. Vanier, *Phys. Rev.* 138, A972–A983 (1965).
9. J. Vanier and C. Audoin, “The Quantum Physics of Atomic Frequency Standards”, Adam Hilger, Bristol, U.K. (1989)



- |   |                             |                            |
|---|-----------------------------|----------------------------|
| 1 -SHOCK MOUNTS                             | 12 -THERMAL SHIELDS         | 24 -SILVERED QUARTZ CAVITY |
| 2 -ION PUMP 270 L/s                         | 13 -TUNING PISTON           | 25 -BULB COLLIMATOR        |
| 3 -PUMP MOUNT                               | 14 -MAGNETIC SHIELDS        | 26 -KINEMATIC MOUNTS       |
| 4 -UHV VALVE                                | 15 -FRAME                   | 27 -THERMAL INSULATION     |
| 5 -SOURCE BULB                              | 16 -OVENS                   | 28 -STATE MIXING COIL      |
| 6 -NECK COIL                                | 17 -GLASS BALLS             | 29 -HEXAPOLE MAGNET        |
| 7 -NECK HEATER                              | 18 -LEAF SPRINGS            | 30 -SOURCE COLLIMATOR      |
| 8 -OVENS                                    | 19 -VACUUM ENCLOSURE        | 31 -SOURCE OSCILLATOR      |
| 9 -TITANIUM PINS                            | 20 -SOLENOID                | 32 -PALLADIUM VALVE        |
| 10 -COUPLING LOOPS                          | 21 -COMPENSATION POSTS      | 33 -HYDROGEN PRESSURE      |
| 11 -QUARTZ STORAGE BULB<br>(TEFLON COATING) | 22 -VAFACTOR TUNER ASSEMBLY | REGULATOR                  |
|   | 23 -TUNING PLATE            | 34 -HYDROGEN CYLINDER      |

Fig. 1. Drawing showing the design features of the masers.

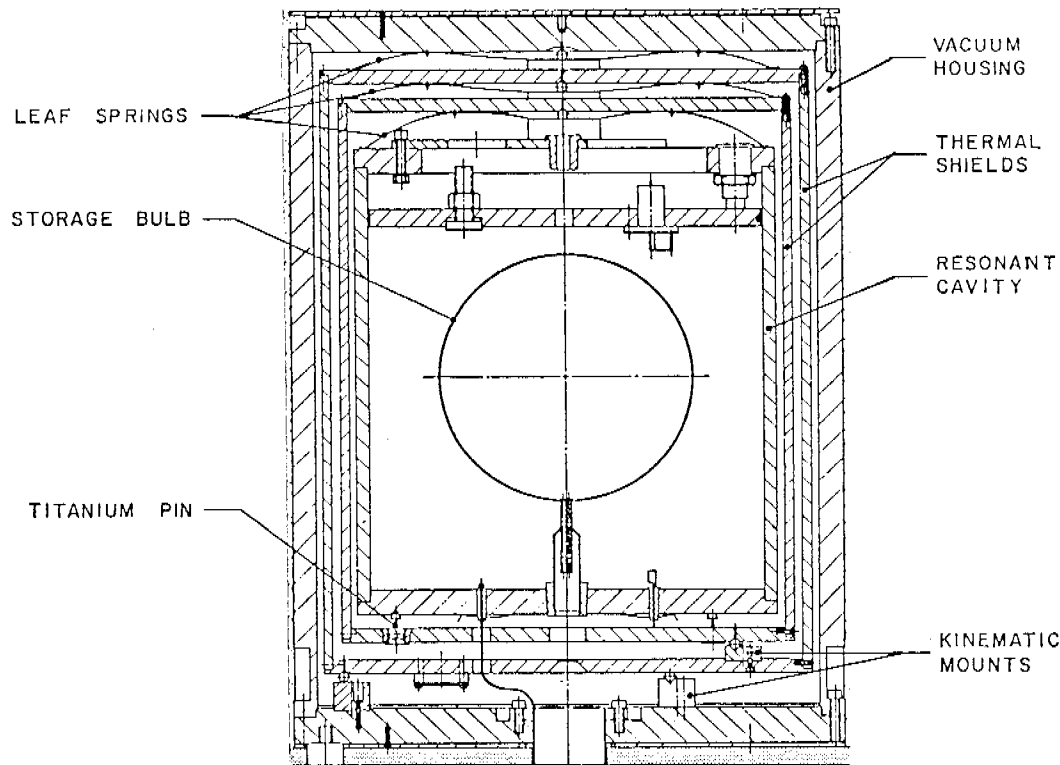


Fig. 2. Detail of cavity region showing thermal shields and kinematic supports.

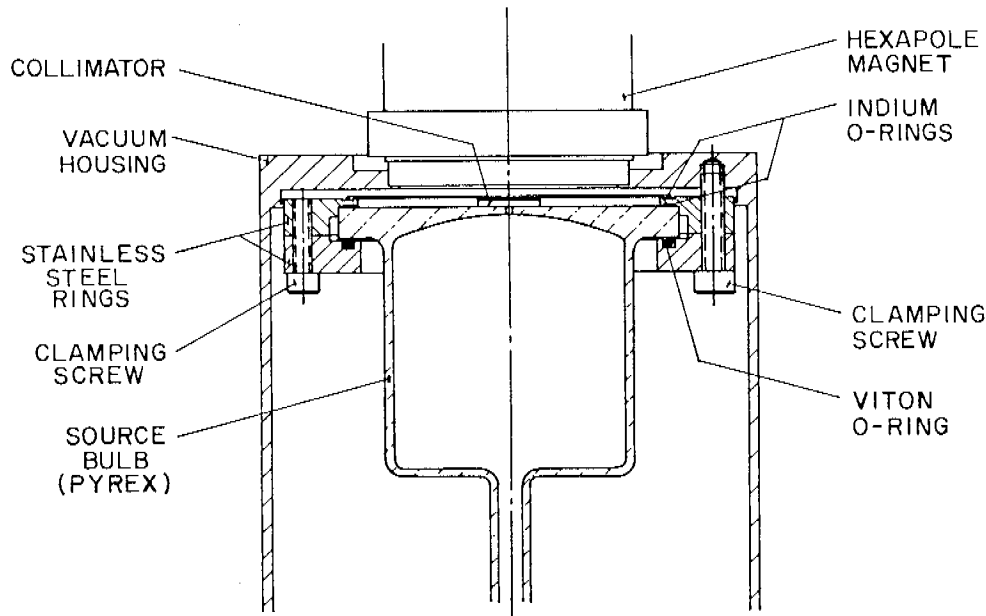


Fig. 3. Detail of vacuum seal to the hydrogen source. The seal is shown in process of assembly.

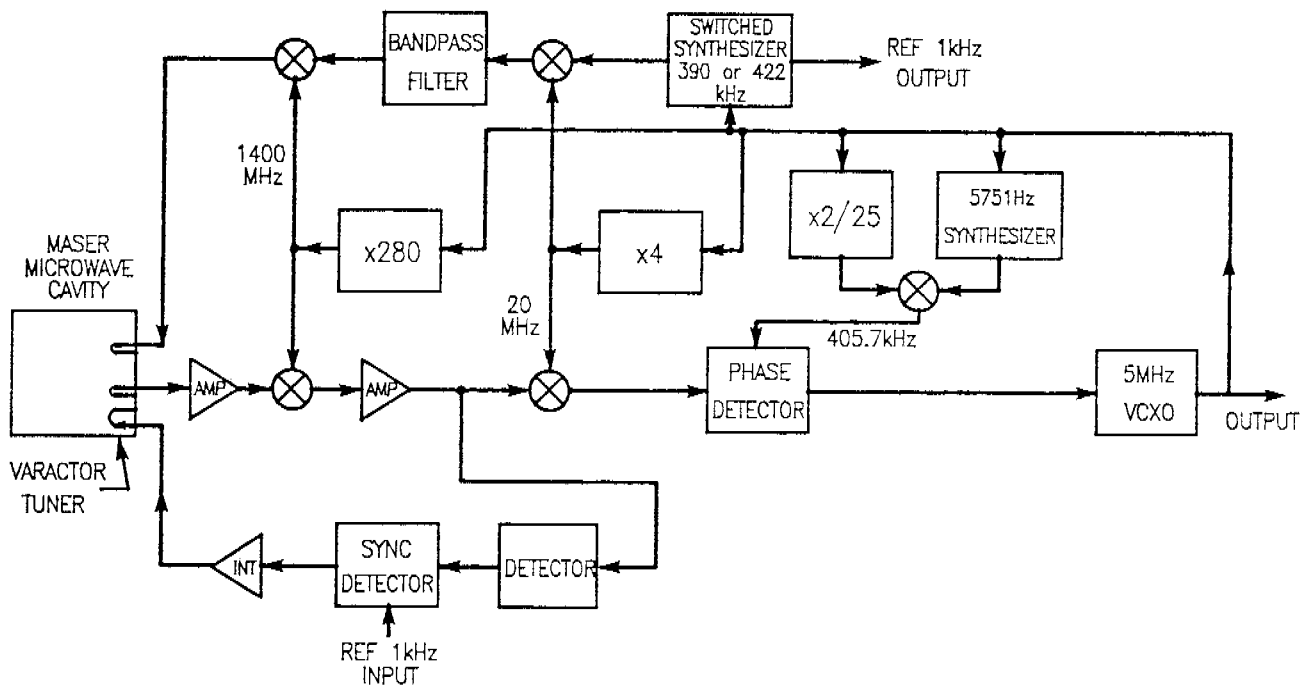


Fig. 4. Simplified block diagram of the maser receiver.

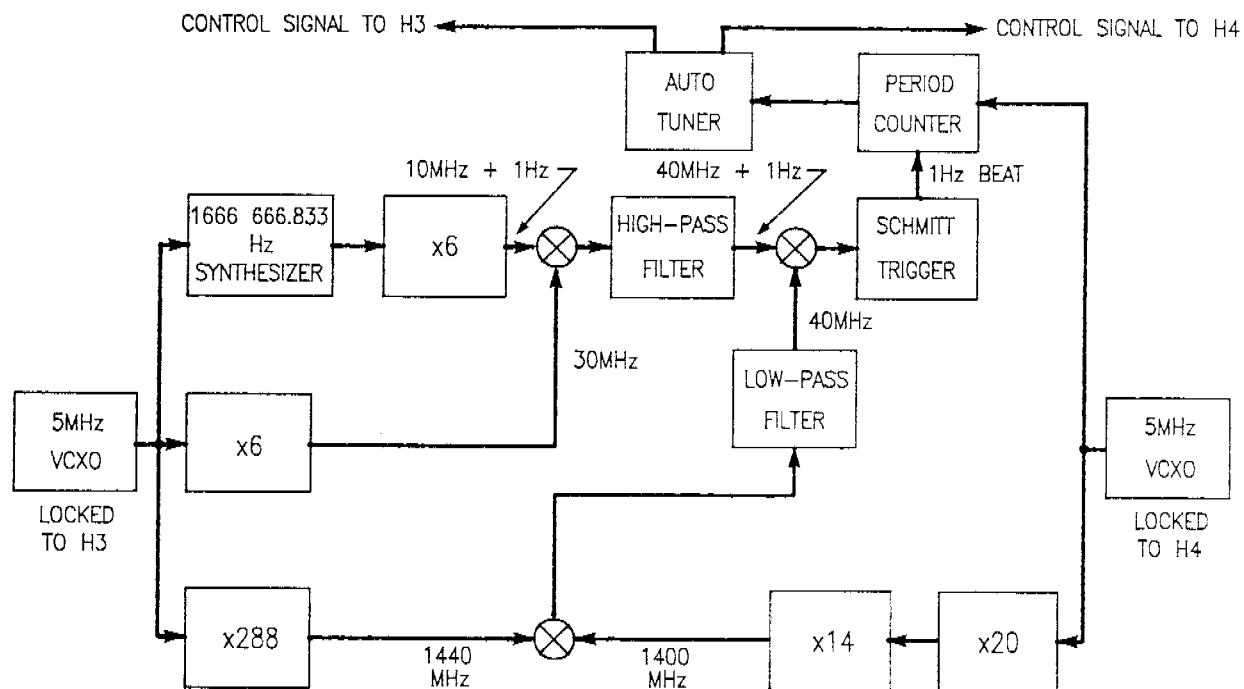


Fig. 5. Block diagram of system designed to produce beats between the masers.

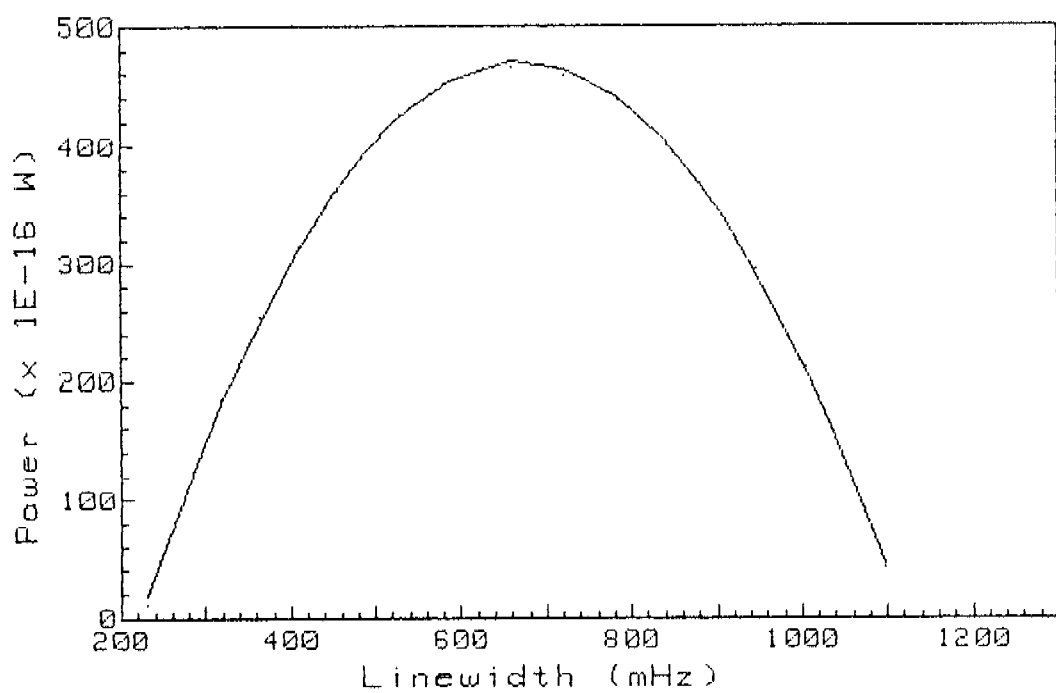


Fig. 6. Output power of maser H4 as a function of linewidth.

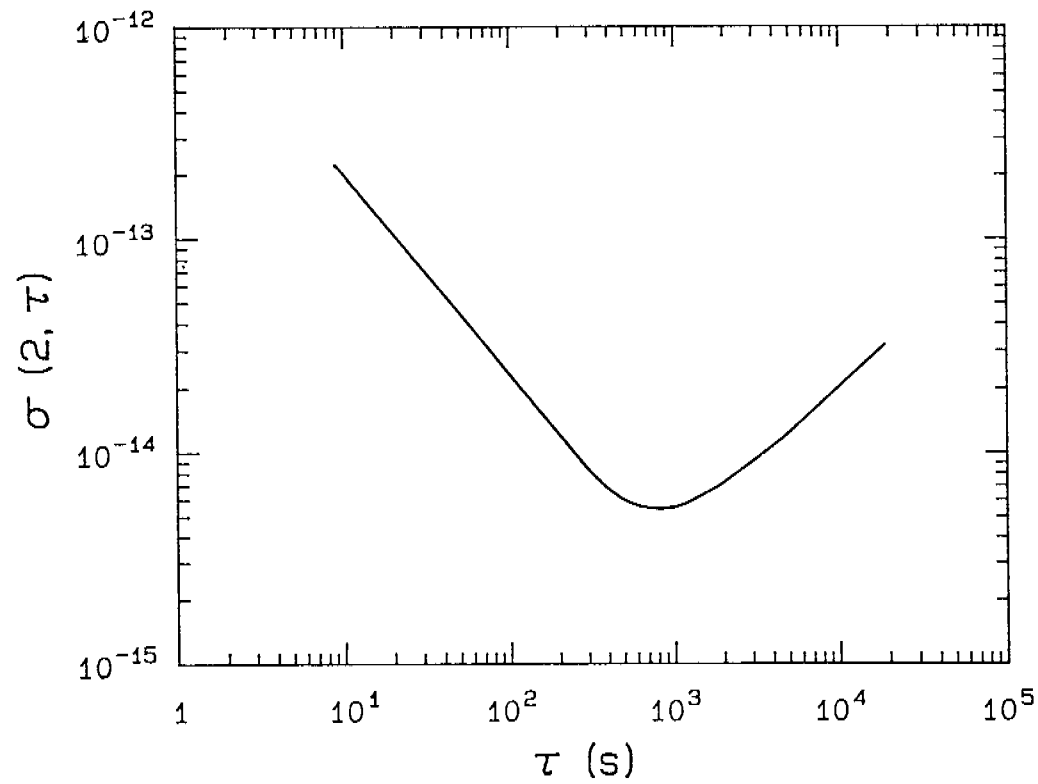


Fig. 7. Preliminary frequency stability data.

## QUESTIONS AND ANSWERS

**ALBERT KIRK, JPL:** How do you introduce the hydrogen into the dissociator bulb and what kind of seal do you use there?

**MR. MORRIS:** We use a palladium leak which is brazed on and then copper seals are used.

**MR. KIRK:** Copper seals between the palladium and the glassware?

**MR. MORRIS:** There is a metal-glass seal and then the stainless steel tubing seal with copper rings seal to the palladium leak.

**FRED WALLS, NIST:** Do you have any magnetic shielding between the source and the state selector and the entrance to the magnetic shields around the cavity?

**MR. MORRIS:** No, we don't. We have a coil that can be activated if necessary in the region between the source and the underside of the magnetic shields. We haven't really had a chance to look at any effects yet, but a quick look at, applying reasonable currents, seemed to show no change in oscillation level.

**DAVID ALLAN, NIST:** The turn up in the  $\sigma$  vs.  $\tau$  curve, was that cavity pulling or do you know what be the cause?

**MR. MORRIS:** We had no temperature control on the masers, there were cables all over the place. It was just to get an initial look at how they were working. We don't have the proper receivers in operation yet, either.